RSC Advances

ROYAL SOCIETY OF CHEMISTRY

www.rsc.org/advances

Journal Name

COMMUNICATION

Fabrication of Rutile TiO_2 Nanorods Arrays on Copper Substrate for High-performance Lithium-ion Batteries

Received 00th January 20xx,
Accepted 00th January 20xx

DOI: 10.1039/x0xx00000x

www.rsc.org/

Guanrao Liu, Shichao Zhang*, Xiaomeng Wu, and Ruoxu Lin

Rutile TiO_2 nanorods array has been successfully prepared on flexible copper substrate and demonstrated as a high-performance anode material for lithium-ion batteries. The prepared materials exhibit excellent electrochemical performance, which depends crucially on the structural parameters of the array and the large specific surface area of the arrays.

To achieve high areal energy and power densities within limited area for next-generation lightweight Li-ion batteries (LIBs), tremendous efforts have been devoted to develop new structured electrode materials.[1-5] It is commonly recognized that titanium dioxide (TiO_2) is a promising anode candidate for fast rechargeable LIBs. Li^+ ion intercalation/de-intercalation in TiO_2-based structures, including anatase, rutile, and TiO_2-bronze (TiO_2-B), are accompanied by negligible lattice changes, which can provide cells with good capacity retention on cycling, low self-discharge and enhanced safety, as well as environmental friendliness.[6-9] Among them, rutile is the thermodynamically most stable structure of TiO_2, and is also the most common natural form. However, bulk rutile can only accommodate <0.1 Li per TiO_2 unit at room temperature,[6, 10] because of anisotropic Li^+ diffusion in rutile structure. As shown in Figure 1, in the *ab*-plane, there is almost no tunnel for Li^+ transport due to the large lattice distortion, but there are channels parallel to the *c*-axis. Several impressive researches achieved to improve the Li^+ intercalation properties of rutile TiO_2 at room temperature, by reducing the particles dimension or solving the problem of irregular aggregation of particles.[10-14]

However, TiO_2 electrodes based on powder materials still suffer from interfacial kinetic problems. The powder need to be mixed with a binder and conductive agent and further pressed onto current collecting substrates before they are suitable for integration into battery devices. This process introduces the additional risks of negating the benefits of electrochemistry using nanomaterials. In addition, efficient electron transport from the current collecting substrate to electrode materials cannot be ensured due to the possible presence of impurities at the interface. To solve these problems, it is an effective way of fabricating nanostructured arrays directly on the metallic current collecting substrates via in situ synthesis, by which the electrode materials possess better homogeneity, mechanical properties, as well as the excellent surface binding strength without any addictive.[15-21] Such kind of arrays combines the advantages of both nanoscaled building blocks and the microstructures, i.e. the electrochemical performance of the electrode can be improved, owing to the high-active surface area, short path for ions, direct transport channel for electrons and specific structure stability. Almost all the reported rutile TiO_2 arrays obtained in solutions were grown on ITO glass, Ti, or some carbon materials, [22-28] which are not suitable for serving as current collector in practice because of the lack of flexibility, limited area or high-cost. Thus, their robust electrochemical applications for LIBs are restricted. In this work, self-supported rutile TiO_2 arrays growing along c-axis fabricated directly on copper current collecting substrates via facile one-step in situ synthesis. The matrials represent an attractive architecture as the electrode of LIBs, owing to the good contact of every nanostructure with the current collector, the high-efficiency of material utilization and the potential of large-area production.

The copper substrate(a thickness of 50μm) for depositing TiO_2 arrays was initially cleaned by sonicating in dilute sulfuric acid (0.5M) and acetone, respectively. The arrays were prepared by hydrothermal treatment of 35mL of $TiCl_3$ (0.15M) solution supersaturated with NaCl as well as 0.3g of urea. The solution was placed in a Teflon-lined autoclave, and the as-cleaned copper substrate was placed in the solution standing against the wall of the autoclave. The autoclave was sealed and maintained at 160 ℃ for 2h. The specimen was immersed in dilute sulfuric acid for 5min and completely washed with distilled water and ethanol for several times. Finally, the sample was dried at 60 ℃ in vacuum oven for 10h.

School of Materials Science and Engineering, Beijing University of Aeronautics and Astronautics, Beijing 100191, P. R. China. Email: csc@buaa.edu.cn
Supplementary Information (ESI) available: [details of any supplementary information available should be included here]. See DOI: 10.1039/x0xx00000x

TiO_2 arrays uniformly are grown on a 6 cm^2 substrate. As is shown from Figure 2a, the shining surface of the copper foil is covered by a piece of white film after hydrothermal treatment. The film can be easily rolled with the substrate, indicating the flexibility of the as-prepared film. Top-surface images of a typical as-synthesized nanorods array sample (Figure 2b) clearly demonstrate a highly uniform and densely packed array of nanorods with tetragonal crystallographic planes. The inset image of Figure 2b is the cross-sectional view of the same sample, clearly demonstrating the large-scale growth of aligned TiO_2 nanorods with typical diameter and length of 100 nm and 800 nm, respectively. Selected area of Figure 2b indicates that the nanorods grow radially from some spots and are self-assembled into micro- and nanoscale hierarchical structures like dandelion. TEM and HRTEM image (Figure 2c and d) of a single rod indicates that the nanorods are well crystallized with clear lattice fringes parallel to the wall. The inter-plane distance is 0.323 nm, which can be indexed as (110) of rutile TiO_2. According to the XRD pattern of the electrode sample, the peaks are attributed to tetragonal rutile-structured TiO_2 (space group $P4_2/mnm$, JCPDS file no.87-710) with the exception of the reflections from the copper substrate. Combined with the XRD data and TEM images, such features imply that the nanorods grow along the *c*-axis with four side surfaces enclosed by {110} planes with a preferred [001] orientation. Energy-dispersive X-ray spectrometry (EDS) analysis (Supporting Information, Figure S1) confirms that the nanorods contain Ti and O without any chloride.

As is known, Ti(III) is not stable in aqueous solution, and easily to be hydrolyzed into $TiOH^{2+}$, which can be oxidized to Ti(IV) by dissolved oxygen in the solution. The hydrolysis reaction of $TiCl_3$ can be described as follows: [22, 28]

$$Ti^{3+} + H_2O \rightarrow TiOH^{2+} + H^+ \quad (1)$$

$$TiOH^{2+} + O_2 \rightarrow \text{Ti(IV) oxo species} + O_2^- \rightarrow TiO_2 \quad (2)$$

The Ti(IV) oxo species is assumed to be an intermediate between TiO^{2+} and TiO_2, consisting of partly dehydrated polymeric Ti(IV) hydroxide.[22-28] The anisotropic growth of 1D titania nanorods can be understood from shape-control chemistry.[29-31] With the formation of a TiO_2 nanocrystal under hydrothermal environment, Cl^- ion can selectively adsorb onto the {110} plane, which suppress and accelerate further growth in the [110] and [001] direction, respectively. Urea can produce ammonia ligands and OH^- by hydroysis in the aqueous solution, which plays an important role here for the growth of nanorods on copper substrate (Details in supporting information, Figure S2): (1) slow down the hydrolysis of Ti^{3+} and afford simultaneously hydrolysis–condensation by olation of the Ti^{3+}, which can control the nucleation progress.[29, 31-33] (2) tailoring the pH value of the reaction solution preventing the corrosion of Cu foils by high concentration of Cl^-,[34, 35] especially with the presence of H^+.

The electrochemical performance of the TiO_2 nanorods arrays on Cu substrate is studied by Swagelok-type two-electrode cells (Details in supporting information).The Cu substrate, which does not alloy with metallic lithium, could function directly as current collectors and the rutile TiO_2 arrays coating acted as the active material so that no other binding or conductive additives were introduced. Note that the accurate mass loading of the active material is difficult to measure because of partial corrosion of Cu substrate thus the capacity unit has to be selected as $\mu Ah \cdot cm^{-2}$.

The cyclic voltammetry (CV) behavior of the prepared electrode in the range of 1 to 2.6 V (vs. Li/Li^+), at a scan rate of 0.1 $mV \cdot s^{-1}$ is depicted in Figure 3a. In the initial cathodic sweep, several characteristic features occur. Li^+ intercalation in single-crystal rutile structures manifests itself by a peak A at ~1.73 V, a small broad peak B at ~1.43V, and an abrupt increase of cathodic current at potentials ~1.1 V (peak C).[36-40] Peak A corresponds to the conversion of TiO_2 into Li_xTiO_2 ($TiO_2+xLi^++xe^-\rightarrow Li_xTiO_2$), and peak A' at ~1.95V represents the extraction of lithium ions from Li_xTiO_2.[36, 37] Peak B and C disappears in the following scans, indicating that there are some irreversible reactions occurring. Solvent degradation is not a significant issue at potentials above 1.0 V, meaning that there is probably a phase transformation in the cycles.[41] Therefore, the absence of peak B and C presumably attributed to the irreversible formation of the $Li_{0.5}TiO_2$ phase from the rutile crystals, which consumes some of the TiO_2 and passivates the interfaces.[38-40] Obviously, the 1D structures of rutile TiO_2 grown along the *c*-axis enhanced the Li^+ diffusion of electrode. In addition, the shapes of CV curves maintained after four cycles, indicating a good cycling performance. Figure 3b displays the galvanostatic discharge /charge curves of the products cycled between 2.6-1.0V at a rate of 5 $\mu A \cdot cm^{-2}$. A total capacity of 386$\mu Ah \cdot cm^{-2}$ is measured at the end of the first discharge, with a reversible capacity of 150 $\mu Ah \cdot cm^{-2}$. During the first discharge, the voltage plateau appeared at 1.73 V (vs. Li/Li^+) corresponding to lithium intercalation into crystalline TiO_2, and the charge potential plateau is observed at around 1.95 V, which are accordant with to the redox peaks in the CV.

The cycling performance of the prepared electrodes was further evaluated. At the current density of 5 $\mu A \cdot cm^{-2}$ and 20 $\mu A \cdot cm^{-2}$(with a reversible specific discharge capacity of 123.6 $\mu Ah \cdot cm^{-2}$), the discharge capacity rentions were 40.4% and 48% from 1st to 2nd cycles respectively, and 38.8% and 37.6% over 50 cycles. (Figure 4a). The arrays exhibit an excellent high rate performance and efficiency when the current density increased to 100 to 200 $\mu A \cdot cm^{-2}$. The reversible capacities of these current density were 91.2 $\mu Ah \cdot cm^{-2}$ and 75.6 $\mu Ah \cdot cm^{-2}$, with barely loss of the capacity after 100 cycles (Figure 4b). The average columbic efficiency is above 95% at 100 $\mu A \cdot cm^{-2}$ and higher rate. Figure 4c depicts the morphologies of rutile TiO_2 nanorods array cycled at current density of 200 $\mu A \cdot cm^{-2}$ after 100 times. The array maintains organized 1D structure, as is known that TiO_2 has no structural change during charge–discharge cycling. Compared to disorderly powder materials, the efficient electron transport from the current collector substrate to electrode materials and the existence of organized 1D morphology with [001] orientation contribute to a homogeneous insertion process.

Conclusions

A self-organized rutile TiO_2 nanorods array is successfully assembled on flexible copper substrate by hydrothermal treatment without any template. The synthesis method is facile, low cost, and highly reproducible. The mechanism of 1D titania nanostructure growth can be understood from shape-control chemistry, by which the array was assembled by nanorods with an organized [001] orientation. The possibility of using this array as active electrode materials for lithium ion batteries was studied. For the metal substrate can be employed as current collector, no polymer binders and conductive agents were used. A specific reversible capacity up to 136 $\mu Ah \cdot cm^{-2}$ is achieved in lithium test cells for as-formed TiO_2 nanorods that were 100 nm in diameter and 800 nm in length. The excellent electrochemical performance depends crucially on the structural properties of the arrays and the good contact of every nanostructure with the current collector, which presents an enormous potential application for LIBs with requirements of lightweight and flexibility.

Acknowledgement

This work was supported by the National Basic Research Program of China (973 Program) (2013CB934001), National Natural Science Foundation of China (51274017), National 863 Program of China (2013AA050904), International S&T Cooperation Program of China (2012DFR60530).

Notes and references

1. M. Armand and J. M. Tarascon, *Nature*, 2008, **451**, 652-657.
2. D. Koziej, A. Lauria and M. Niederberger, *Adv. Mater.*, 2014, **26**, 235;
3. N. Liu, Z. Lu, J. Zhao, M. T. McDowell, H. W. Lee, W. Zhao and Y. Cui, *Nat. Nanotechnol.*, 2014, **9**, 187-192.
4. H. Wang and H. Dai, *Chem. Soc. Rev.*, 2013, **42**, 3088-3113.
5. H. Li and H. Zhou, *Chem. Commun.*, 2012, **48**, 1201-1217.
6. T. Ohzuku, Z. Takehara, and S. Yoshizawa, *Electrochim. Acta,* 1978, **24**, 219-222.
7. A. R. Armstrong, G. Armstrong, J. Canales, R. García, and P. G. Bruce, *Adv. Mater.*,2005,**17**, 862-865.
8. G. F. Ortiz, I. Hanzu, T. Djenizian, P. Lavela, J. L. Tirado, and P. Knauth, *Chem. Mater.* 2009, **21**, 63-67.
9. X. Y. Yu, H. B. Wu, L. Yu. F. X. Ma, and X. W. Lou , *Angew. Chem. Int. Edit.*,2015, **54**, 4001-4004.
10. L. Kavan, D. Fattakhova, and P. Krtil, J. Electrochem. Soc., 1999, **146**, 1375-1379
11. Y. S. Hu, L. Kienle, Y. G. Guo, and J. Maier, *Adv. Mater.*, 2006, **18**, 1421-1426.
12. N.A. Milne, M. Skyllas-Kazacos, and V. Luca, *J. Phys. Chem. C*, 2009, **113**, 12983-12995.
13. J. S. Chen, and X. W. Lou, *J. Power Sources*, 2010, **195**, 2905-2908.
14. X. Li, C. M. Zhang and T. Meng, *RSC Adv.*, 2016, **6**,4321-4328
15. L. Kavan, M. Kalbac, M. Zukalova, I. Exnar, V. Lorenzen, R. Nesper, and M. Graetzel, *Chem. Mater.*,2004, **16**, 477-485.
16. J. P. Liu, Y. Y. Li, X. T. Huang, R. M. Ding, Y. Y. Hu, J. Jiang, and L. Liao, *J. Mater. Chem.*, 2009, **19**, 1859-1864
17. Y. S. Jung, A. S. Cavanagh, L. A. Riley, S. H. Kang, A. C. Dillon, M. D. Groner, S. M. George, S. H. Lee, *Adv. Mater.*, 2010, **22**, 2172-2176.
18. T. Djenizian, I. Hanzu, P. Knauth, *J. Mater. Chem.,* 2011, **21**, 9925-9937.
19. B. Han, S. C. Zhang, R. Zhou, X. M. Wu, X. Wei, Y. L Xing, S. B. Wang, and T. Qi, *RSC Adv*. ,2014, **4**,50752–50758
20. K. Cheng, F. Yang, K. Ye, Y. Zhang, X. Jiang, J. L. Yin, G. L. Wang, and D. X. Cao, *J. Power Sources*, 2014, **258**, 260 - 265
21. Q. Li, X. G. Miao, C. X. Wang, and L. W. Yin, *J. Mater. Chem. A*, 2015, **3**, 21328-21336
22. E. Hosono, S. Fujihara, K. Kakiuchi, and H. Imai, *J. Am. Chem. Soc.*, 2004, **126**, 7790-7791.
23. X. G. Peng, L. Manna, W. D. Yang, E. S. Wickham, A. Kadavanich, and A. P. Alivisatos, *Nature*, 2000, **404**,59-61.
24. A. S. Barnard, and L. A. Curtiss, *Nano Lett*., 2005, **5**, 1261-1266.
25. X. J. Feng, K. Shankar, O. K. Varghese, M. Paulose, T. J. Latempa, and C.A. Grimes, *Nano Lett*., 2008, **8**, 3781-3785.
26. S. M. Dong, H. B. Wang, L. Gu, X. H. Zhou, Z. H. Liu, P. X. Han, Y. Wang, X. Chen, G. L. Cui, L. Q. Chen, *Thin Solid Films*, 2011, **519**, 5978–5982
27. L. F. He, R. G. Ma, N. Du, J. G. Ren, T. L. Wong, Y. Y. Li, S. T. Lee, *J. Mater. Chem.,* 2012, **22**, 19061–19066
28. W. X. Guo, C. Xu, X. Wang, S. H. Wang, C. F. Pan,C. J. Lin, and Z. L. Wang, *J. Am. Chem. Soc.,* 2012, **134**, 4437 – 4441
29. L. Vayssieres, and M. Graetzel, *Angew. Chem. Int. Ed*., 2004, **43**, 3666-3670.
30. H. Wang, Z. Chen, Y. Leung, C. Luan, C. Liu, Y. Tang, C. Yan, W. Zhang, J. A. Zapien, I. Bello, and S. Lee, *Appl. Phys. Lett.,* 2010, **96**, 263104-2603106,
31. Y. B. Zhang, X. J. Feng, L. Jiang, *Sci. China Ser. B-Chem.,* 2007, **50**, 175-178
32. Y. H. Jin, S. H. Lee, H. W. Shim, K. H. Ko, and D. W. Kim. *Electrochim. Acta,* 2010, **55**, 7315-7321
33. K. C. Song, Y. Kang, *Mater. Lett.*, 2000, **42**, 283-289.
34. Lei, J. L.; Li, L. J.; Cai, S. M.; Zhang, S. T.; Li, D., Yang, M. Z. *Acta Phys. -Chim. Sin.*, 2001, **17**, 1101-1111.
35. Nunez, L.; Reguera, E., Corvo, F.; Gonzalez, E.; Vazquez, C. *Corros. Sci.*, 2005, **47**, 461-484.
36. D.H. Wang, D.W. Choi, Z.G. Yang, V. V. Viswanathan, Z. M. Nie, C. M. Wang, Y. J. Song, J. G. Zhang, and J. Liu, *Chem. Mater.,* 2008, **20**, 3435-3442.
37. J. S. Chen, Y. L. Tan, C. M. Li, Y. L. Cheah, D. Y. Luan, S. Madhavi, F. Y. C. Boey, L. A. Archer, and X. W. Lou, *J. Am. Chem. Soc.* 2010,**132**, 6124-6130.
38. Z. Hong, M. Wei, T. Lan, L. Jiang, and G. Cao, *Energy Environ. Sci*. 2012, **5**, 5408-5413.
39. K. Siwinska-Stefanska, and B. Kurc, *J. Power Sources*, 2015, **299**, 286-292.
40. M. Marinaro, M. Pfanzelt, P. Kubiak, R. Marassi, and M. Wohlfahrt-Mehrens, *J. Power Sources,* 2011, **196**, 9825-9829 .
41. M. V. Koudriachova, N. M. Harrison, and S. W. Leeuw, *Phys. Rev. Lett*., 2001, **86**, 1275-1278.

Journal Name

COMMUNICATION

Figure Caption

Figure 1. Structural representation of rutile along the (a) [100], and (b) [001] directions. The octahedra are representative of TiO_6

Figure 2. (a) Optical image, (b) top-view and Inset in (b) shows an cross section of the array, (c) TEM image of single rod and (d) HRTEM images of the rods. (e) Corresponding XRD pattern of the nanorods array.

Figure 3. (a) CV test conducted between 1.0-2.6V with a scan rate of $0.1mV{\cdot}s^{-1}$ arrows across the curves indicates direction of increasing cycle number; (b) Discharge–charge voltage profiles at the $5\mu A{\cdot}cm^{-2}$ for the first to fifth cycles.

Figure 4. (a) and (b) Cycling performance at various current density for nanorods array with cut-off voltage of 1.0 -2.6 V, (c) Top view and side view of the sample after 100 discharge/charge cycles at $200mA{\cdot}cm^{-2}$

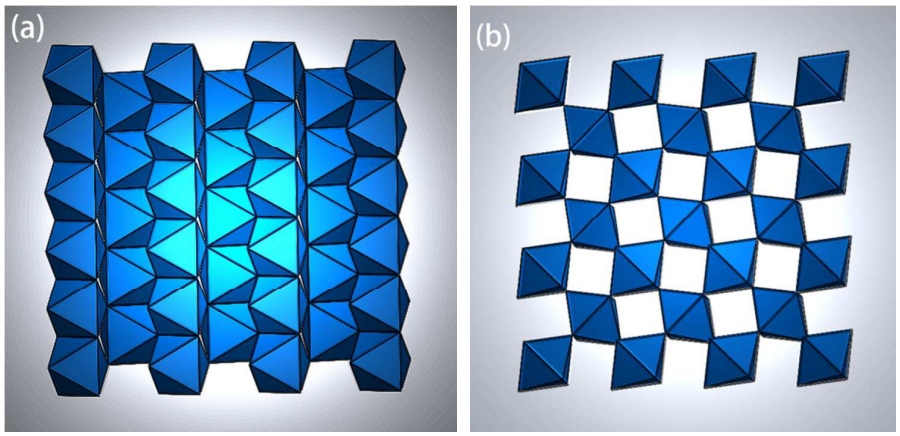

Figure 1. Structural representation of rutile along the (a) [100], and (b) [001] directions. The octahedra are representative of TiO_6

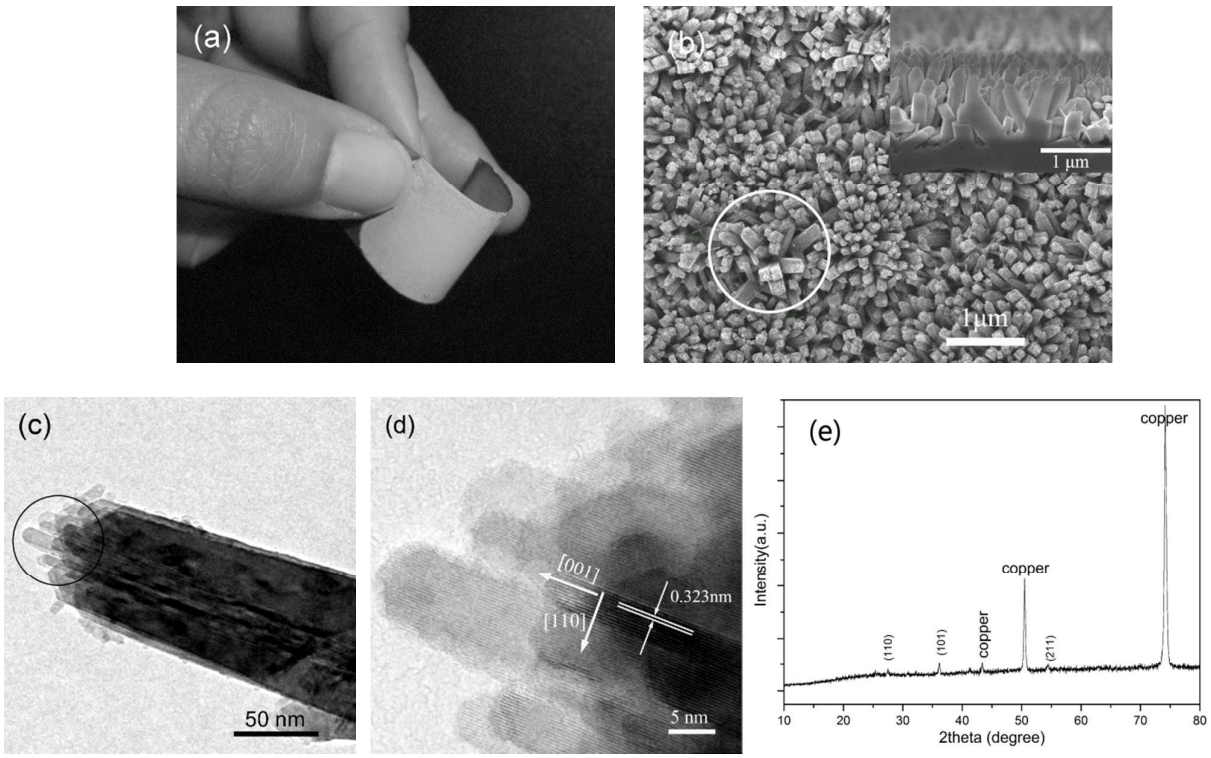

Figure 2. (a) Optical image, (b) top-view and Inset in (b) shows an cross section of the array, (c) TEM image of single rod and (d) HRTEM images of the rods. (e) Corresponding XRD pattern of the nanorods array.

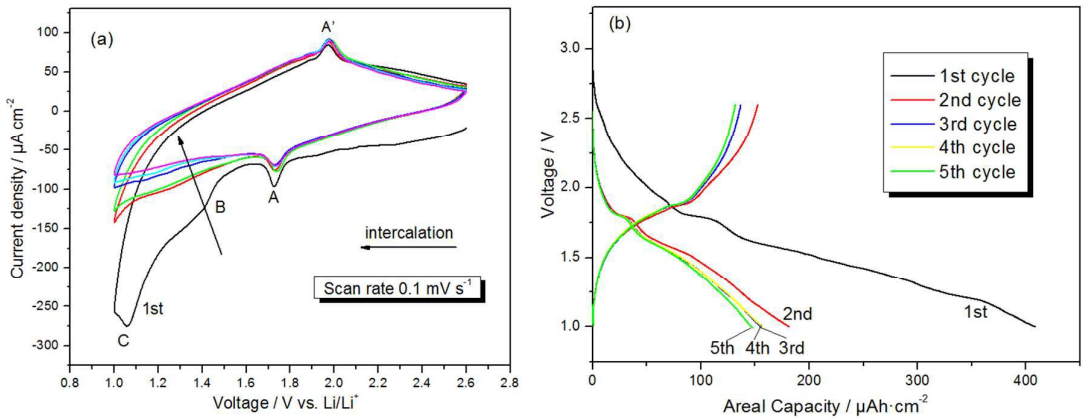

Figure 3. (a) CV test conducted between 1.0-2.6V with a scan rate of 0.1mV·s^{-1} Arrows across the curves indicates direction of increasing cycle number; (b) Discharge–charge voltage profiles at the 5μA·cm^{-2} for the first to fifth cycles.

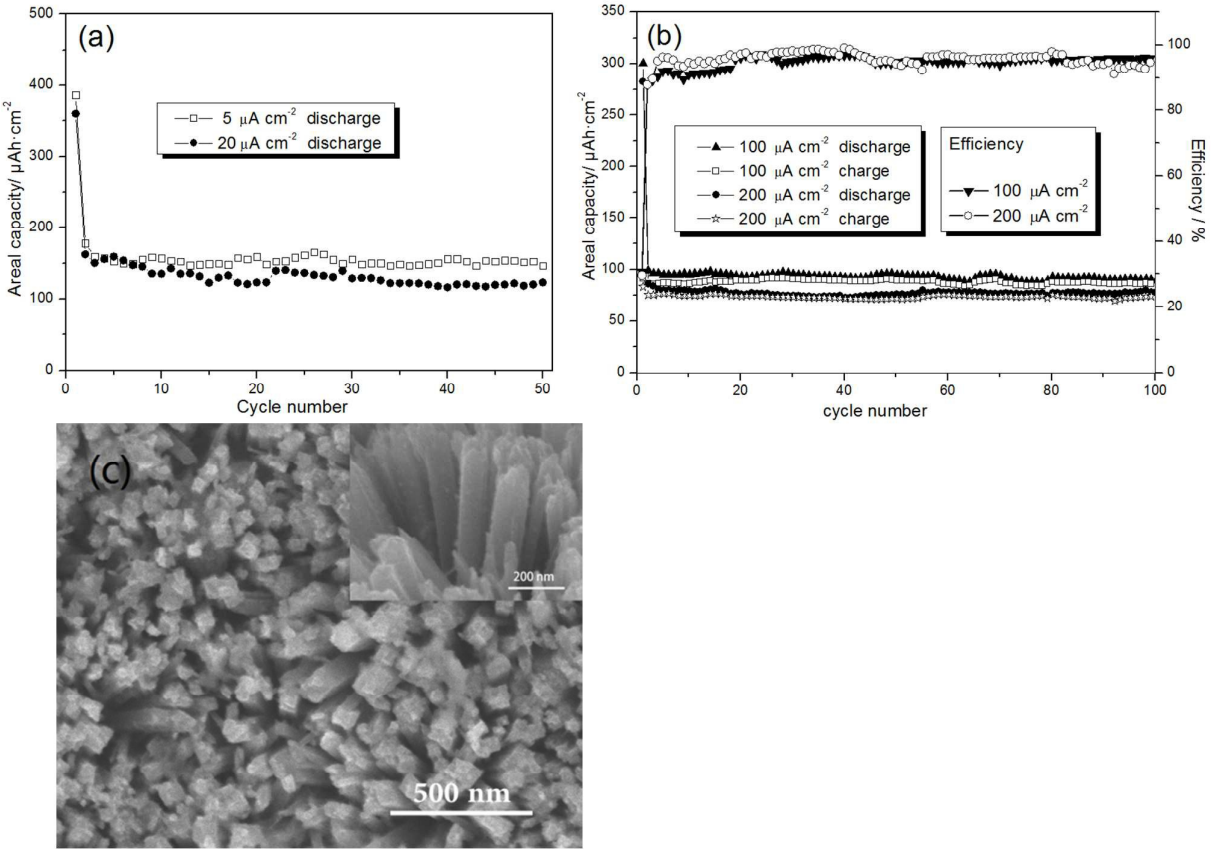

Figure 4. (a) and (b) Cycling performance at various current density for nanorods array with cut-off voltage of 1.0 -2.6 V; (c) Top view and side view of the sample after 100 discharge/charge cycles at 200mA·cm^{-2}

Graphical Abstract

TiO_2 nanorods array has been prepared directly on flexible copper substrate via in situ synthesis, presenting enormous potentials in LIBs.